ChemPubSoc Europe

DOI: 10.1002/cphc.201601262

CHEMPHYSCHEM Articles

Ce^{IV}–Gd^{III} Mixed Oxides as Hosts for Er^{III}-Based Upconversion Phosphors

Cecilia Sorbello,[a] Petra Gross,[b] Cristian A. Strassert,[c] Matías Jobbágy,*[a] and Beatriz C. Barja*[a]

A family of Er^{III} and Er^{III}–Yb^{III} based nanophosphors, hosted in monophasic oxidic Ce^{IV}–Gd^{III} binary solid solutions, was prepared. The samples were formulated with a constant Er^{III} content as the activator, with the eventual addition of Yb^{III} as a sensitizer. The amorphous $Ce_{0.94-x}Gd_xEr_{0.06}(OH)CO_3{\cdot}H_2O$ and $Ce_{0.94-x}Gd_xEr_{0.05}Yb_{0.01}(OH)CO_3{\cdot}H_2O$ precursors were prepared by following the urea method to obtain monodispersed spheres of tunable size ranging from 30 to 450 nm. After being decomposed at 1273 K under an atmosphere of air, the precursors of 200 nm in diameter evolved into monophasic polycrystalline particles preserving the parent shape and size. The role of the composition of the binary matrices in the emission properties was evaluated for two different excitation wavelengths (976 nm and 780 nm) based on the upconversion (UC) emission spectra and their dependence on the incident power. The yield of the UC process is discussed in the framework of established and novel alternative mechanisms. The number of vacancies and mainly the symmetry of the Er^{III} environment play major roles in the deactivation pathways of the UC emission mechanisms. However, the colours obtained by employing bare Ce^{IV} or Gd^{III} hosts are preserved in the related monophasic Ce^{IV}-rich or Gd^{III}-rich binary hosts.

1. Introduction

Inorganic luminescent particles are being used in an increasing number of applications beyond the traditional uses related to display technologies. Soft chemistry synthetic routes allowed the preparation of novel luminescent phases textured in the form of size-tuned micro- or even nanometric particles[1–3] that are suitable for signalling and imaging of biological systems.[4,5] As an alternative to conventional high-energy excitation, the process of photon upconversion (UC) employs non-harmful long-wavelength excitation and emits visible output radiation.[6] The majority of compounds that can undergo UC involve trivalent lanthanides, Ln^{III}, because these centres have more than one metastable level, with excited-state lifetimes typically in the range of 10^{-6}–10^{-2} s, being the basic requirement for UC.[6,7] Given that 4 f electrons are well shielded from their chemical environment by the outer 5 s and 5 p electrons, a particularly small electron–phonon coupling strength for the various excited f-f states results. As a consequence, luminescence processes are much more competitive than multiphonon relaxation in lanthanides, as compared with other centres. Lanthanides have been hosted within several matrices such as fluorides,[8–10] oxides,[11,12] phosphates,[13] and vanadates.[14] Certain rare-earth (RE) based oxides such as CeO_2[15,16] or Gd_2O_3[17–19] offer highly biocompatible hosts for Er^{III}-based UC phosphors, with relevant biomedical functionalities.[20–25]

It is known that, for a given host matrix such as Gd_2O_3 or CeO_2, changes in the proportion of activator and sensitizer ions Er^{III}/Yb^{III} leads to different emission colours; with red emission being favoured for higher levels of sensitizer. The question regarding how would changes in the composition of a binary Ce^{IV}-Gd^{III} oxide matrix at a fixed Er^{III}/Yb^{III} ratio impact the luminescent properties of these phosphors was not fully addressed. To our knowledge, no reports dealing with binary hosts of different composition for upconversion phosphors have been published. Beyond the applications, these binary hosts offer interesting inherent crystallochemical properties, not found in other Ce^{IV}-RE^{III} systems. The Ce^{IV}-Gd^{III} binary oxides develop solid solutions in a wide range of compositions, evolving from an eight-fold coordination environment (CeO_2 lattice) to a six-fold one (Gd_2O_3 lattice). The incorporation of Gd^{III} results in an extremely small change of the lattice constant.[26] In addition to the nearest neighbour environment, the particle size and shape also affect the luminescence performance,[27–29] making the control of these variables mandatory for comparative studies. Recent attempts to obtain Ce^{IV}-Gd^{III} oxidic hosts resulted in nanoparticles with extremely different size and shapes.[30] More recently, we employed the urea method[31–36] for the preparation of a family of Ce^{IV}-Gd^{III} oxidic particles to host Eu^{III} centres.

[a] Dr. C. Sorbello, Dr. M. Jobbágy, Dr. B. C. Barja
Departamento de Química Inorgánica Analítica y
Química Física FCEyN-Universidad de Buenos Aires, INQUIMAE-CONICET
Ciudad Universitaria Pabellón 2
C1428EHA, CABA (Argentina)
E-mail: jobbag@qi.fcen.uba.ar
barja@qi.fcen.uba.ar

[b] Dr. P. Gross
Institute for Physics, Carl von Ossietzky University
Carl-von-Ossietzky-Str. 9, 26129 Oldenburg (Germany)

[c] Priv.-Doz. Dr. C. A. Strassert
Physikalisches Institut and Center for Nanotechnology (CeNTech)
Westfälische Wilhelms-Universität Münster, Heisenbergstraße 11
48149 Münster (Germany)

Supporting Information for this article can be found under: http://dx.doi.org/10.1002/cphc.201601262.

The method ensured well-defined textural properties (size, shape and monodispersion) along the whole range of Ce^{IV}-to Gd^{III} ratio.[25]

In this work, a systematic preparation and characterization of UC phosphors based on representative Ce^{IV}-Gd^{III} oxidic solid solutions is presented. We observed that different CIE colours can be obtained for different proportions of the components of a binary host because of changes in the number of vacancies and symmetry of the Er^{III} environment, keeping the level of activator Er^{III} and sensitizer Yb^{III} ions constant.

Samples were formulated with a fixed content of Er^{III} with the eventual addition of Yb^{III} as sensitizer. The role of the matrix in the emissive properties of the samples was evaluated at two different excitation wavelengths (976 nm and 780 nm) based on the UC emission spectra and their dependence on the incident power.

2. Results and Discussion

2.1. Synthesis and Characterization of the Samples

The synthetic method employed herein allows the preparation of almost any RE^{III} solid solution in the form of weakly crystallised $RE(OH)CO_3{\cdot}H_2O$,[37] also known as amorphous phase. The method enables monodispersed spheres of diameters ranging from several nanometres to microns to be obtained, depending on the preparation protocol, with quantitative yield.[25] Similar $RE(OH)CO_3{\cdot}H_2O$ monodispersed particles can be quantitatively obtained as a function of the initial reagents concentrations (see Figure S1 in the Supporting Information). Concerning the chemical composition, these precursors allow a continuous degree of substitution, independent of the employed RE^{III}, due to their inherently similar hydrolytic chemistry, ensuring their quantitative coprecipitation. Typically, if only stable RE^{III} cations such as Gd^{III} are employed, pure RE_2O_3 oxides are obtained. However, if an aliovalent cation such as Ce^{III} prevails in the precursor's composition, formation of a CeO_2-like (F_m3_m) phase is to be expected.[38] In the present case, the Ce^{III} to Gd^{III} ratio was chosen according to our previous report, to ensure the formation of monophasic $Ce_{1-x}RE_xO_{2-x/2}$ (F_m3_m) or $RE_{2-x}Ce_xO_{3+x/2}$ (I_3a) phases, exclusively.[25] Under these conditions, oxide particles of 200 ± 20 nm were obtained. Table 1 compiles the cation content for the prepared samples as well as the corresponding sample codes.

Table 1. Labels, composition (expressed as atomic percentage of cations), space group and cell parameter of the samples.

	Ce^{III}	Gd^{III}	Er^{III}	Yb^{III}	Cell	*a* [Å]
C0E	–	94	6	–	I_3a	10.794(2)
C10E	10	84	6	–	I_3a	10.830(4)
C84E	84	10	6	–	F_m3_m	5.4198(5)
C94E	94	–	6	–	F_m3_m	5.411(1)
C0EY	–	94	5	1	I_3a	10.788(8)
C10EY	10	84	5	1	I_3a	10.810(2)
C84EY	84	10	5	1	F_m3_m	5.417(1)
C94EY	94	–	5	1	F_m3_m	5.411(1)

A smooth baseline recorded on the PXRD of all precursors confirmed the expected amorphous $RE(OH)CO_3{\cdot}H_2O$ nature (data not shown).[39] Once these precursors were decomposed and annealed at 1273 K under air atmosphere, well-defined diffraction patterns were observed (see Figure 1). Samples prepared with bare Gd^{III} and $Ce^{IV}_{0.1}Gd^{III}_{0.9}$ hosts exhibited a *c*-type (I_3a) structure related to the Gd_2O_3 lattice, including characteristic 411, 332 and 134 reflections placed in the range of $34 < 2theta < 44$. Samples prepared with bare Ce^{IV} and $Ce^{IV}_{0.9}Gd^{III}_{0.1}$ hosts exhibited a F_m3_m-type (CeO_2) structure.

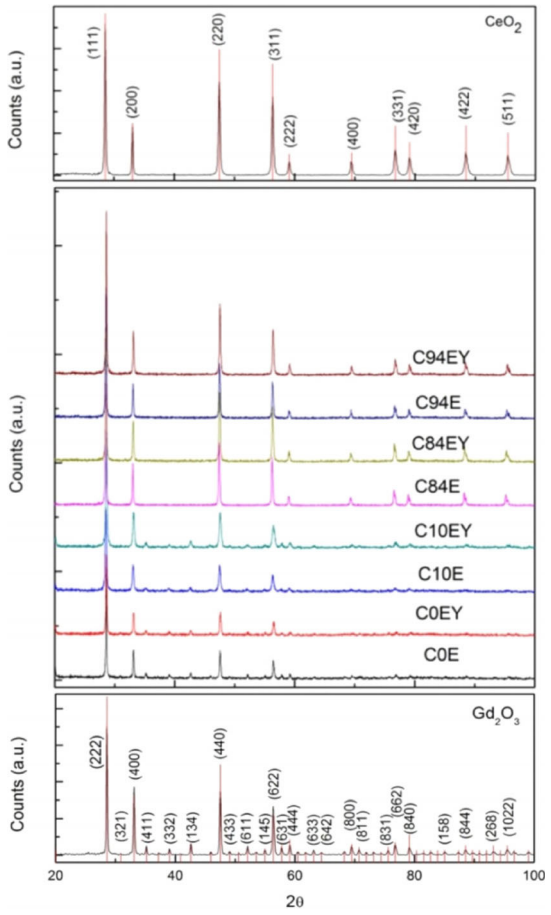

Figure 1. PXRD patterns of the samples (main panel centre). Indexed patterns for the crystallographic reference of bare Gd_2O_3 (PDF#65-3181, lower panel) and bare CeO_2 (PDF#65-2975, upper panel) obtained under similar conditions are also included.

Table 1 compiles the cell parameters of the observed cubic cells; all the observed values are in good agreement with the Gd^{III}-Ce^{IV} reference oxides.[26,40,41] The observed net cell contraction corresponds to the smaller Shannon's ionic radii of Er^{III} and Yb^{III} (0.89 and 0.868 Å in a six-fold coordination, respectively) as compared with Gd^{III} (0.938 Å).[42]

The absolute deviations found for *a* cell parameters of F_m3_m samples with respect to bare CeO_2 are in good agreement with RE^{III}-substituted CeO_2 phases in the solid solution condition (see Figure S2 in the Supporting Information).[43,44] HRSEM-assisted examination of the samples revealed a common textural evolution during the annealing, irrespective of composi-

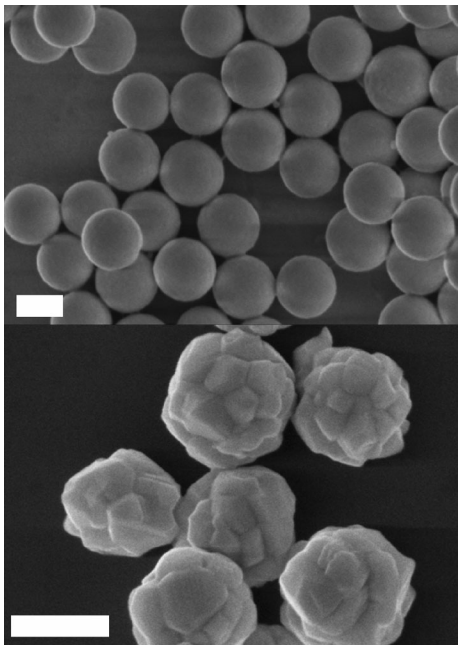

Figure 2. HRSEM images of the amorphous precursor of sample C84E (upper image) and the corresponding material after annealing (lower image). The scale bar represents 200 nm in both images.

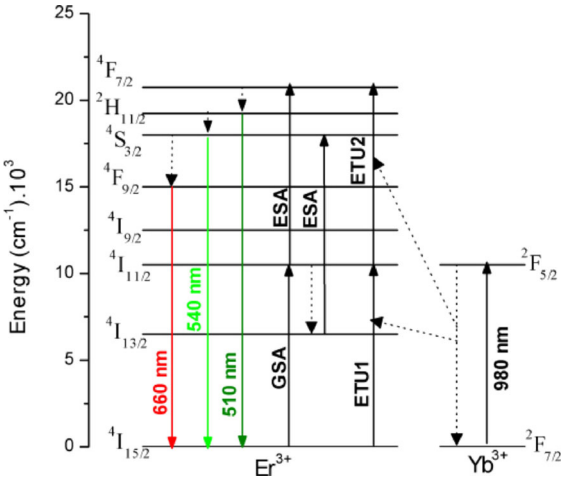

Scheme 1. Energy levels of Er^{III} and Yb^{III} centres and the possible transitions under 976 nm excitation.

tion. The parent spherical particles of cuasi amorphous basic carbonates evolved into polycrystalline contracted faceted spheroids, constituted by strongly coalesced crystallites of 20–60 nm. However, no massive interparticle sintering was developed, allowing a significant preservation of both shape and size of the parent precursors (see Figure 2 and S3 in the Supporting Information).[33,45,46]

2.2. Luminescence Properties

2.2.1. Upconversion Spectra

The accepted mechanisms to populate the excited states in systems with many electronic states are the GSA (ground-state absorption) with subsequent ESA (excited-state absorption) and/or ETU (energy transfer UC) processes. ESA is a single-centre process independent of the Er^{III} concentration, whereas ETU is strongly dependent on the distance between the centres involved in the process. Thus, both the host matrix structure and the Er^{III} concentration are relevant: the higher the latter, the more probable the ETU process becomes.[47,48] Scheme 1 shows the energy level diagram for the Yb^{III}/Er^{III} co-doped system showing the main UC processes responsible for the green and red emission upon excitation at 976 nm.[49] The Yb^{III} centre acts as a sensitizer due to its larger absorption cross section at 976 nm ($^2F_{7/2}\rightarrow{}^2F_{5/2}$) and the excellent energy matching with the energy difference of the two levels ($^4I_{15/2}\rightarrow{}^4I_{11/2}$) of the Er^{III}. The energy absorbed by Yb^{III} is transferred to the Er^{III} centres by ETU, enabling the $^4I_{15/2}\rightarrow{}^4I_{11/2}$ transition of the Er^{III}. A second ETU process can further promote the Er^{III} centres to the higher $^4F_{7/2}$ level to decay by multiphonon relaxations to the $^2H_{11/2}/^4S_{3/2}$ state, from which green light is emitted, or can alternatively relax to the $^4F_{9/2}$ to emit in the red range. In the absence of Yb^{III}, the $^4I_{11/2}$ of Er^{III} level is populated through GSA from the ground $^4I_{15/2}$ level by a 976 nm photon followed by multiphonon relaxation to the $^4I_{13/2}$ state. A second 976 nm photon populates the $^4F_{7/2}$ level of the same Er^{III} centre through ESA process, or it can accept energy from another Er^{III} centre in the matrix through an ETU process (not shown). The luminescent emitting levels $^4F_{9/2}$ (red-range light) and $^2H_{11/2}$, $^4S_{3/2}$ (green range light) can be populated by multiphonon relaxation from the upper level $^4F_{7/2}$. The predominance of one mechanism over the other depends on the degree of substitution and on the nature of the matrices, particularly on their phonon energies.

Figure 3 shows the UC emission spectra of the samples by exciting at 976 nm or 780 nm. The spectrum of each sample shows the two groups of bands in the red and green regions corresponding to the following Er^{III} transitions: the bands in the green region (530–570 nm) are assigned to the $^2H_{11/2}/^4S_{3/2}\rightarrow{}^4I_{15/2}$ transitions, whereas those in the red region (640–690 nm) are assigned to the $^4F_{9/2}\rightarrow{}^4I_{15/2}$ transition.

No blue emission was observed in the present samples, irrespective of their composition. Only green and red UC emission has been reported for Er^{III}-Yb^{III} hosted in bare CeO_2, either by excitation at 976 or 780 nm.[50] In the case of Er^{III} hosted in bare Gd_2O_3, blue UC emission was recorded by excitation with green lasers.[51]

Upon excitation at 976 nm, the Gd^{III}-rich matrices (C0E, C0EY, C10E and C10EY) emit predominantly in the red region. In contrast, the Ce^{IV}-rich matrices (C84E, C84EY, C94E and C94EY) show an enhancement of the green emission (see figures and Table S1 in the Supporting Information). The addition of Yb^{III} increases the red to green emission ratio for all samples, in agreement with the previous results observed for Er^{III}-Yb^{III} hosted in bare CeO_2[16] and Gd_2O_3 nanocrystals.[18] In the aforementioned cases, the increase of the red emission was achieved either by increasing the Yb^{III} or Er^{III} content. In the present study, what generates the change in this ratio is not the Er^{III} or Er^{III}-Yb^{III} content, which is fixed for all the samples, but

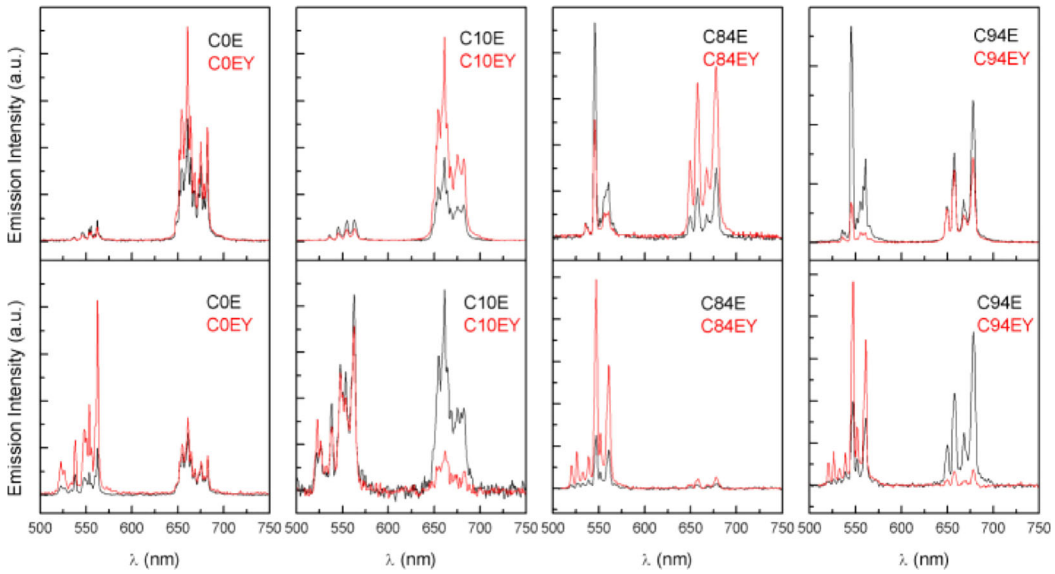

Figure 3. UC emission spectra of the samples for $\lambda_{exc}=976$ nm (top) and 780 nm (bottom) recorded at 65 mW.

the change in the composition of the binary host. If the C10E and C84E samples are compared, the red to green ratio are 4.4 and 0.8, respectively. These ratios grow to 17.8 and 5.1 for the C10EY and C84EY samples. When the samples are excited at 780 nm, only Er^{III} can absorb with a prevailing green emission in all cases, irrespective of the addition of Yb^{III}. This suggests that Yb^{III} offers a new path that deactivates the red emission of Er^{III}. The Er^{III} is excited by GSA to the $^4I_{9/2}$ state, from which it can decay non radiatively to the $^4I_{11/2}$ and $^4I_{13/2}$ levels before it absorbs a second photon to reach the $^2H_{11/2}$ or $^4S_{3/2}$ states.[52] The $^4I_{11/2}$ level matches the excited state $^2F_{5/2}$ of Yb^{III}, which can accept the energy transferred from the Er^{III} centres before the red emission occurs. For each sample, the overall emission colour, either employing $\lambda_{exc}=976$ nm or 780 nm, was defined based on CIE chromaticity coordinates; the resulting colours are directly displayed in Table 2 for clarity.

Table 2. CIE coordinates for the CXE and CXEY series excited with $\lambda_{exc}=976$ nm and for $\lambda_{exc}=780$ nm, employing an 80 mW nominal power.

Sample	$\lambda_{exc}=780$ nm	$\lambda_{exc}=976$ nm
C0E	$X=0.3809$	$X=0.4770$
	$Y=0.5839$	$Y=0.4106$
C10E	$X=0.3557$	$X=0.4221$
	$Y=0.6073$	$Y=0.4611$
C84E	$X=0.3153$	$X=0.3421$
	$Y=0.6457$	$Y=0.6492$
C94E	$X=0.3817$	$X=0.3530$
	$Y=0.5814$	$Y=0.5983$
C0EY	$X=0.3412$	$X=0.5337$
	$Y=0.5913$	$Y=0.3569$
C10EY	$X=0.3131$	$X=0.5106$
	$Y=0.6595$	$Y=0.3699$
C84EY	$X=0.3084$	$X=0.4370$
	$Y=0.6734$	$Y=0.5018$
C94EY	$X=0.3121$	$X=0.4622$
	$Y=0.6621$	$Y=0.4915$

Comparing the emission spectra obtained by one-photon excitation (see Figures S4–5, in the Supporting Information) with the UC spectra of the samples excited at 976 nm, the green bands are always favoured over the red bands. If the emissive $^4S_{3/2}$ and $^4F_{9/2}$ levels of Er^{III} were populated exclusively by a multistep nonradiative relaxation from the higher $^2H_{11/2}$ level, the intensity ratio of the green to red emission should be the same regardless the excitation mechanism (Stokes or anti-Stokes). If not, other energy transfer processes must be involved in the UC emission to populate the $^4F_{9/2}$ level to enhance the red emission over the green emission at $\lambda_{exc}=976$ nm.

2.2.2. Power Dependence Studies

To gain insights into the UC mechanisms that populate the emissive excited states $^4F_{9/2}$ (red light) and $^2H_{11/2}$ or $^4S_{3/2}$ (green light), it is mandatory to measure the dependence of the emission intensities, I, of the emitted visible light as a function of the incident pump power, P. For a sequential absorption of n photons, the intensity of the emitted light and the incident power obeys the equation: $I \approx P^n$.[53] The UC emission spectra of the samples were measured for increasing excitation powers ($\lambda_{exc}=976$ nm) at the main emission wavelengths (see Figures S6–7 in the Supporting Information). The logarithmic dependence of the intensity of the main emission bands in the green and red range with the incident power ($\lambda_{exc}=976$ nm) for all samples excluding C84E and C84EY is shown in Figure 4.

For most of the samples, it is observed that the values of n are lower than 2, which would correspond to a two-photon excitation process, irrespective of the monitored emission wavelength. These low values of n can be interpreted in terms of the competition between the linear decay and the UC mechanisms responsible for the depletion of the intermediate excited states as documented in detail by Pollnau et al.[53] The intensity of the luminescence and the incident power depends directly

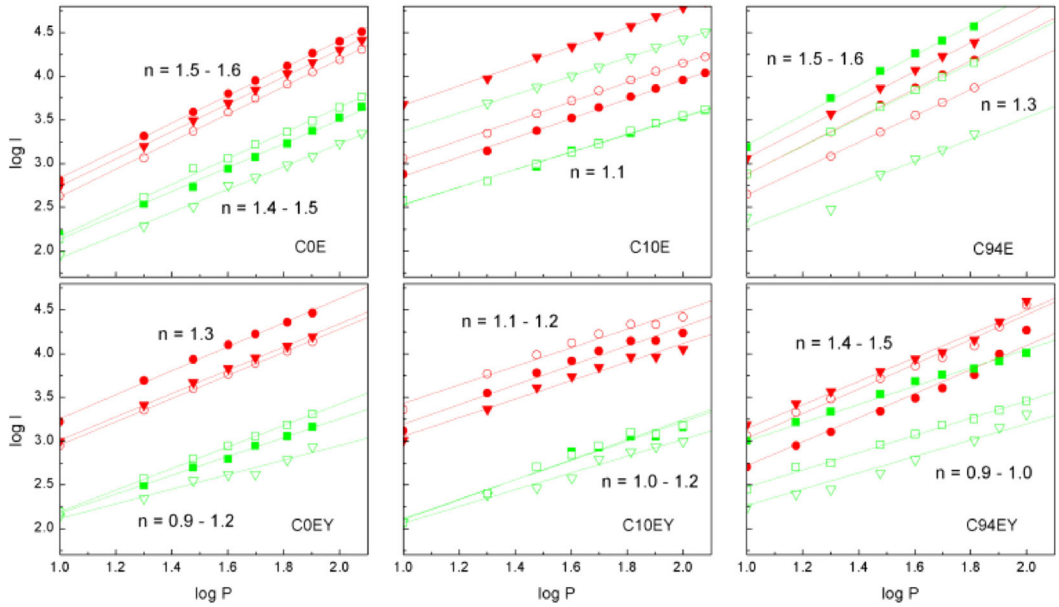

Figure 4. Logarithmic dependence of the intensity of the main UC emission bands as a function of the input power (λ_{exc} = 976 nm), including the estimated slopes, *n*, recorded at 535–546 nm (empty triangles), 545–555 nm (filled squares), 555–562 nm (empty squares), 649–661,5 nm (filled circles), 661–675 nm (empty circles), and 675–682 nm (filled triangles). See Table S2, in the Supporting Information, for specific values of each sample.

on the way in which the intermediate level is depleted. If the depletion of the intermediate level is linear and dominates over the UC mechanisms, the slope *n* is closer to 2. If the opposite occurs, the *n* values are closer to 1. This behaviour has already been observed for Er^{III} hosted within bare CeO_2[16] or Gd_2O_3[17,19] nanocrystals. In the present case, the intermediate levels responsible for the green ($^4I_{11/2}$) and the red emission ($^4I_{13/2}$) are mainly depleted by UC mechanisms.

The dependence of the intensity of the main emission bands with the incident power for samples C84E and C84EY are shown in Figure 5, denoting significant differences with respect to the other samples. For similar incident power intervals, all the red emitted wavelengths (649.5, 675.5, 678.0 and 682.0 nm) change their slopes at log *P* = 1.7 (C84EY) and at log *P* = 1.9 (C84E) to 3.3 and 3.9, respectively, to recover the initial value (C84EY). These large values have no physical meaning in terms of a strict two-photon process and strongly suggest that a feedback mechanism must be taking place to populate the level $^4F_{9/2}$ involved in the red emission. A photon avalanche process would explain these results. However, high pump powers are usually needed to start the process and the time to achieve a proper number of cycles is much longer than the lifetimes of the excited states involved in the system. Goldner et al.[54] proposed a mechanism called CRESA (cross-relaxation enhanced excited state absorption) as an alternative process to conventional photon avalanche in which resonant GSA is used to initiate the looping cycles. In the frame of that mechanism, we propose the following sequence (see Scheme 2). First, by excitation at 976 nm the Yb^{III} centres are sequentially excited to the $^2F_{5/2}$, which transfers the energy by two ETU to the Er^{III} centres, resulting in excited Er^{III} $^4F_{7/2}$ centres. These excited Er^{III} $^4F_{7/2}$ centres relax by multiphonon relaxation

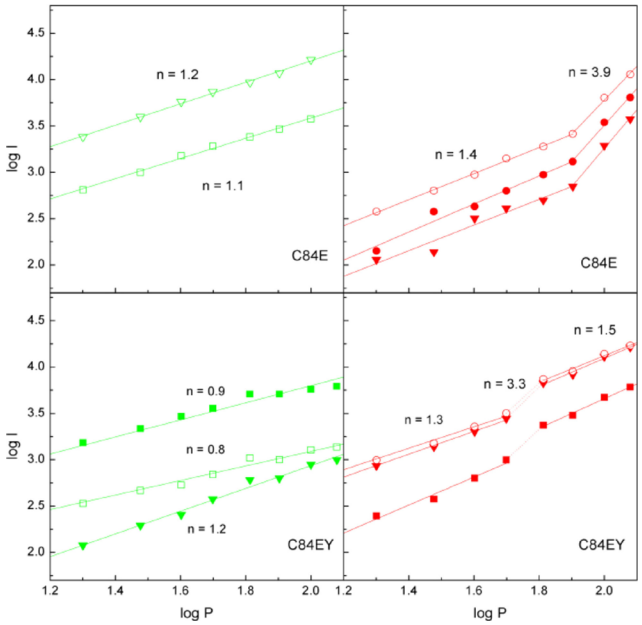

Figure 5. Logarithmic dependence of the emitted intensity of the main UC emission bands as a function of the input power (λ_{exc} = 976 nm), including the estimated slopes, *n*, recorded at 535,5–546 nm (filled green triangles), 545–555 nm (filled green squares), 555–562 nm (empty green squares), 649–661.5 nm (filled red circles and squares), 661–675 nm (empty red circles), and 675–682 nm (filled red triangles). See Table S3, in the Supporting Information, for specific values of each sample.

to the Er^{III} $^2H_{11/2}$ (or $^4S_{3/2}$). A multiphonon-assisted cross relaxation (CR) then takes place as shown in Equation (1):

$$Er^{III}\ ^2H_{11/2} + Yb^{III}\ ^2F_{7/2} \rightarrow Er^{III}\ ^4I_{11/2} + Yb^{III}\ ^2F_{5/2} \quad (1)$$

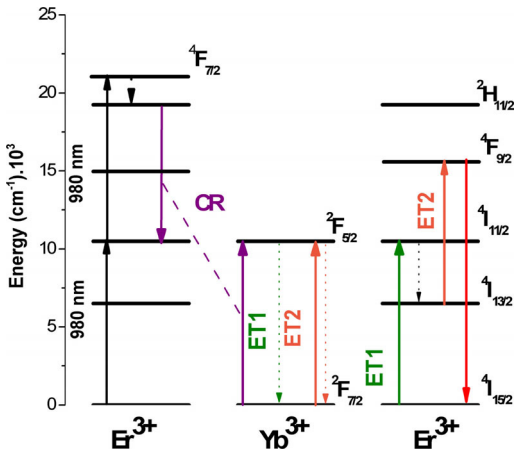

Scheme 2. Energy diagram for the UC mechanism proposed for the samples C8E and C84EY.

This process is facilitated by the matrix in which three phonons can approximately cover the 1200–1100 cm^{-1} gap. The excited Yb^{III} $^2F_{5/2}$ transfers its energy to another Er^{III} $^4I_{15/2}$ to populate the excited Er^{III} $^4I_{11/2}$. The result of this process is described by Equation (2):

$$Er^{III}\ ^2H_{11/2} + Er^{III}\ ^4I_{15/2} \rightarrow 2\ Er^{III}\ ^4I_{11/2} \quad (2)$$

In this mechanism, the Er^{III} $^4I_{11/2}$ centres are always regenerated because of the energy transfer from the Yb^{III} $^2F_{5/2}$ to the Er^{III} $^4I_{11/2}$, resulting in a feedback process. The red emission is obtained when the excited Er^{III} $^4I_{11/2}$ relaxes to the long living Er^{III} $^4I_{13/2}$ level through multiphonon relaxation to immediately be excited to the $^4F_{9/2}$ through energy transfer from the Yb^{III} $^2F_{5/2}$ centres.

The intermediate $^4I_{13/2}$ level for red emission is being depleted by UC mechanisms, in agreement with the slopes observed in the log*I* vs. log*P* plots in Figure 5. No feedback mechanism seems to take place in the green emission region in view of the small and constant values of *n*. A similar anomalous power dependence of UC emission was already reported for Er^{III} (1–10%) hosted in Gd_2O_3 nanocrystals upon excitation at 976 nm.[55] However, this anomaly was not observed once these nanocrystals were annealed at higher temperatures, suggesting a key contribution of lattice defects to its occurrence. The authors proposed a closed positive UC looping to explain the observed multiphoton processes, based on a limiting case of a CRESA mechanism. Sivakumar et al.[56] also described this mechanism as hetero looping enhanced energy transfer (Hetero-LEET).

Upon excitation at 780 nm, where Yb^{III} cannot absorb, no changes in the slopes were observed (see Figures S8–10 and Table S4, in the Supporting Information) either in the green or in the red regions. At this wavelength, the sensitizer does not absorb and the $^2F_{5/2}$ state of Yb^{III} offers an alternative deactivation path and therefore no regeneration of the $^4I_{11/2}$ of Er^{III} is observed. This result indicates that the Yb^{III} centres are involved in the cooperative mechanism when the samples are excited at 976 nm where its role as a sensitizer is fundamental.

Considering that in these series the shape and size of the particles are similar and the Er^{III} content is invariant, the differences in the emission processes can only be ascribed to the variable compositions of the hosts. In the present case, for Ce^{IV}-rich hosts (C94E, C94EY C84E, C84EY), the substitution of the parent Ce^{IV} cations by any RE^{III} generates oxygen vacancies[57] within the parent lattice with a consequent change in the symmetry of the system. Recent NMR based studies revealed that when Y^{III} ions are incorporated within CeO_2 hosts, most of them locate in a wide range of sevenfold oxygen environments whereas a smaller fraction is positioned in the more symmetric eightfold oxygen environment.[58,59]

Complementary emission studies also reported this behaviour for Eu^{III}[60] or Sm^{III}[61] hosted in CeO_2. Then, a prevalence of variable sevenfold environments for both Er^{III} and Yb^{III} cations is expected in the ceria rich samples, given the similarities in their radii with Y^{III} and Eu^{III}. Both experimental[62] and in silico[57] studies agree that oxygen vacancies tend to permanently associate with RE^{III} ions smaller than Gd^{III}. Given that this is the case for Er^{III} and Yb^{III} ions, the contribution of the mobile oxygen vacancies to the emission properties of the samples seems to be less preponderant than the change in the symmetry of their sites.

In contrast, Gd^{III} hosts (C0E, C0EY) offer a defined sixfold coordination environment resulting from the isomorphic substitution with either Er^{III} or Yb^{III}, as was previously reported.[55] In the case of samples C10E and C10EY, a small fraction of sevenfold environments can be expected.

The occurrence of sudden changes in the slopes of the log*I* vs. log*P* plots for the C84E and C84EY in the red region can be ascribed to a maximum in the environment asymmetry, in line with the reports dealing with ill-crystallised related hosts.[54–56] Additionally, the dynamic measurements showed that C84E presents the lowest lifetime decay in the red region ($^4F_{9/2}$): τ_{C84E} (22.9 μs) $< \tau_{C94E}$ (28.1 μs) $< \tau_{C10E}$ (34.0 μs) $< \tau_{C0E}$ (43.5 μs) as expected for lower symmetry sites.

The samples C84E and C84EY are the CeO_2-like matrices with the maximum number of vacancies because of the highest RE^{III} substitution. The oxygen vacancies can migrate in the matrix, generating new states with energies (ca. 520 nm) that overlap the green emission states of the Er^{III} ($^2H_{11/2}$, $^4S_{3/2}$), offering a new deactivation path in these ceria-like matrices.[62] This fact is in line with the results observed in the log*P* vs. log*I* plots in which no feedback process was evidenced in view of the lack of sudden slope changes.

3. Conclusions

Application of the urea method combined with a suitable thermal treatment allows quantitative preparation of well-defined crystalline monophasic Er-Yb-Gd-Ce oxidic spheroidal phosphors of 200 nm. Different CIE colours were obtained by changing the proportions of the components of a binary host for a fixed level of activator and sensitizer ions. The number of vacancies and mainly the symmetry of the Er^{III} environment play a major role in the deactivation pathways of the UC emission mechanisms. However, the colours obtained by employing

bare hosts (C0E/EY and C94E/EY samples) are preserved in the related monophasic binary hosts (C10E/EY and C84E/EY samples).

Experimental Section

Synthesis and Characterization of the Samples: The precursors were prepared by following the urea method[25] by aging several solutions containing Ce^{III} nitrate hexahydrate, Gd^{III} nitrate hexahydrate, Er^{III} nitrate pentahydrate and Yb^{III} nitrate pentahydrate with a total cation content of (1.5×10^{-2} mol dm^{-3}) and urea (0.5 mol dm^{-3}), ensuring quantitative coprecipitation of all cations, as confirmed by ICP analysis. The final ratios for each RE^{III} to ($[Ce^{III}]+[Gd^{III}]+[Er^{III}]+[Yb^{III}]$), were expressed as *%RE*, are presented in Table 1. Typically, 50 mL of each solution were filtered, bubbled with nitrogen and aged at 363 K for 3 h. After quenching the reaction in an ice bath, the solids were filtered (0.2 μm membranes), washed with water and dried at RT overnight. Mixed oxides (phosphors) were synthesised by heating the precursors for 6 h at 1273 K under an air atmosphere, at a 5 K min^{-1} rate. All synthesised precursors and the resulting oxides were characterised by powder X-ray diffraction (PXRD) using the graphite-filtered Cu Kα radiation ($\lambda=1.5406$ Å), with a step size of 0.02 and 2 s step time. The cell parameters were estimated from the main reflections recorded between $20<2$ *theta* <100. HRSEM was performed on samples straight deposited onto conductive silicon wafer substrates without further metallization.

Steady-State Luminescence Measurements: Emission/excitation corrected spectra were recorded with a Horiba Jobin Yvon Spectrofluorometer (Fluorolog 3) equipped with a 450 W Xenon lamp (230–1800 nm) and a TBX-04 photomultiplier tube module (response 185–650 nm).

Upconversion Measurements: Upconversion measurements were performed by optical excitation at 976 nm or at 780 nm. Radiation at 976 nm was supplied by a continuous-wave, fibre-coupled laser diode (3S Photonics). The fibre output was collimated with a lens of 11-mm focal length, and a second lens with 25-mm focal length was used to adjust the spot size on the powder sample inside a glass capillary. A 20× microscope objective with 0.4 NA was used to collect the upconverted radiation under a small detection angle of $<45^\circ$. The residual excitation laser light was removed from the detection path by using a short-pass filter with a cut-off wavelength of 850 nm; the upconverted light was coupled into a transport fibre leading to a spectrometer (Stellarnet EPP2000). For excitation of the sample at 780 nm, the diode laser was replaced with a titanium sapphire laser (Coherent Micra) supplying pulsed radiation with a 60 fs pulse. The light was focused onto the sample through a lens with 25 mm focal length, and the light was collected by using the same 20× MO before being coupled to the same spectrometer. Residual excitation light was filtered through a short-pass filter with a cut-off wavelength of 700 nm. Emission spectra were corrected considering the inherent response of the employed detector. The CIE (Commission Internationale de l'Eclairage-1934) chromaticity coordinates of the samples were calculated by employing the ColorCalculator software, freely provided by OSRAM-Sylvania website.

Acknowledgements

This work was supported by the University of Buenos Aires (UBACyT 20020130100610BA), the Agencia Nacional de Promoción Científica y Tecnológica (ANPCyT PICT 2012-1167) and Consejo Nacional de Investigaciones Científicas y Técnicas (CONICET PIP 11220110101020). C.S. acknowledges CONICET for a doctoral fellowship. B.B. and M.J. are Research Scientist of CONICET (Argentina). B.C.B. thanks to the Deutscher Akademischer Austausch Dienst (DAAD) for the financial support received for an international research exchange within the Scientific and Technological Cooperation Program (Argentine-Germany).

Conflict of interest

The authors declare no conflict of interest.

Keywords: energy transfer · lanthanides · luminescence · photochemistry · solid-state structures

[1] K. Sooklal, B. S. Cullum, S. M. Angel, C. J. Murphy, *J. Phys. Chem.* **1996**, *100*, 4551–4555.
[2] G. S. Yi, H. C. Lu, S. Y. Zhao, G. Yue, W. J. Yang, D. P. Chen, L. H. Guo, *Nano Lett.* **2004**, *4*, 2191–2196.
[3] B. M. Tissue, *Chem. Mater.* **1998**, *10*, 2837–2845.
[4] F. Wang, D. Banerjee, Y. S. Liu, X. Y. Chen, X. G. Liu, *Analyst* **2010**, *135*, 1839–1854.
[5] D. K. Chatterjee, A. J. Rufaihah, Y. Zhang, *Biomaterials* **2008**, *29*, 937–943.
[6] M. Haase, H. Schafer, *Angew. Chem. Int. Ed.* **2011**, *50*, 5808–5829; *Angew. Chem.* **2011**, *123*, 5928–5950.
[7] F. Wang, X. Liu, *Chem. Soc. Rev.* **2009**, *38*, 976–989.
[8] F. Wang, X. G. Liu, *J. Am. Chem. Soc.* **2008**, *130*, 5642–5643.
[9] D. Chen, Y. Zhou, Z. Wan, Z. Ji, P. Huang, *Dalton Trans.* **2015**, *44*, 5288–5293.
[10] D. Chen, M. Xu, P. Huang, *Sens. Actuators B* **2016**, *231*, 576–583.
[11] F. Vetrone, J. C. Boyer, J. A. Capobianco, A. Speghini, M. Bettinelli, *Chem. Mater.* **2003**, *15*, 2737–2743.
[12] A. Patra, C. S. Friend, R. Kapoor, P. N. Prasad, *J. Phys. Chem. B* **2002**, *106*, 1909–1912.
[13] S. Heer, O. Lehmann, M. Haase, H. U. Gudel, *Angew. Chem. Int. Ed.* **2003**, *42*, 3179–3182; *Angew. Chem.* **2003**, *115*, 3288–3291.
[14] Y. J. Sun, H. J. Liu, X. Wang, X. G. Kong, H. Zhang, *Chem. Mater.* **2006**, *18*, 2726–2732.
[15] S. Babu, J.-H. Cho, J. M. Dowding, E. Heckert, C. Komanski, S. Das, J. Colon, C. H. Baker, M. Bass, W. T. Self, S. Seal, *Chem. Commun.* **2010**, *46*, 6915–6917.
[16] J. H. Cho, M. Bass, S. Babu, J. M. Dowding, W. T. Self, S. Seal, *J. Lumin.* **2012**, *132*, 743–749.
[17] L. Xu, Y. Yu, X. Li, G. Somesfalean, Y. Zhang, H. Gao, Z. Zhang, *Opt. Mater.* **2008**, *30*, 1284–1288.
[18] H. Guo, N. Dong, M. Yin, W. P. Zhang, L. R. Lou, S. D. Xia, *J. Phys. Chem. B* **2004**, *108*, 19205–19209.
[19] Y. Q. Lei, H. W. Song, L. M. Yang, L. X. Yu, Z. X. Liu, G. H. Pan, X. Bai, L. B. Fan, *J. Chem. Phys.* **2005**, *123*, 174710.
[20] S. Setua, D. Menon, A. Asok, S. Nair, M. Koyakutty, *Biomaterials* **2010**, *31*, 714–729.
[21] J.-G. Li, X. Li, X. Sun, T. Ishigaki, *J. Phys. Chem. C* **2008**, *112*, 11707–11716.
[22] J. Chen, S. Patil, S. Seal, J. F. McGinnis, *Nat. Nanotechnol.* **2006**, *1*, 142–150.
[23] E. G. Heckert, A. S. Karakoti, S. Seal, W. T. Self, *Biomaterials* **2008**, *29*, 2705–2709.
[24] A. Karakoti, S. Singh, J. M. Dowding, S. Seal, W. T. Self, *Chem. Soc. Rev.* **2010**, *39*, 4422–4432.

[25] C. Sorbello, B. C. Barja, M. Jobbagy, *J. Mater. Chem. C* **2014**, *2*, 1010 – 1017.
[26] C. Artini, M. Pani, M. M. Carnasciali, M. T. Buscaglia, J. R. Plaisier, G. A. Costa, *Inorg. Chem.* **2015**, *54*, 4126 – 4137.
[27] L. F. Hu, R. Z. Ma, T. C. Ozawa, T. Sasaki, *Angew. Chem. Int. Ed.* **2009**, *48*, 3846 – 3849; *Angew. Chem.* **2009**, *121*, 3904 – 3907.
[28] C. Wu, W. Qin, G. Qin, D. Zhao, J. Zhang, S. Huang, S. Lü, H. Liu, H. Lin, *Appl. Phys. Lett.* **2003**, *82*, 520 – 522.
[29] A. Vecht, C. Gibbons, D. Davies, X. Jing, P. Marsh, T. Ireland, J. Silver, A. Newport, D. Barber, *J. Vac. Sci. Technol. B* **1999**, *17*, 750 – 757.
[30] H. Qiu, G. Chen, R. Fan, C. Cheng, S. Hao, D. Chen, C. Yang, *Chem. Commun.* **2011**, *47*, 9648 – 9650.
[31] G. Soler-Illtia, M. Jobbagy, R. J. Candal, A. E. Regazzoni, M. A. Blesa, *J. Dispersion Sci. Technol.* **1998**, *19*, 207 – 228.
[32] E. Matijevic, W. P. Hsu, *J. Colloid Interface Sci.* **1987**, *118*, 506 – 523.
[33] B. Aiken, W. P. Hsu, E. Matijevic, *J. Am. Ceram. Soc.* **1988**, *71*, 845 – 853.
[34] T. C. Rojas, M. Ocana, *Scr. Mater.* **2002**, *46*, 655 – 660.
[35] M. Jobbágy, C. Sorbello, E. E. Sileo, *J. Phys. Chem. C* **2009**, *113*, 10853 – 10857.
[36] Y. Tian, B. Tian, C. Cui, P. Huang, L. Wang, B. Chen, *RSC Adv.* **2015**, *5*, 14123 – 14128.
[37] Z. C. Kang, L. Eyring, *J. Solid State Chem.* **1990**, *88*, 303 – 323.
[38] A. Nakamura, K. Imai, N. Igawa, Y. Okamoto, E. Yamamoto, S. Matsukawa, M. Takahashi, *Hyperfine Interact.* **2012**, *207*, 67 – 71.
[39] M. Jobbágy, F. Marino, B. Schönbrod, G. Baronetti, M. Laborde, *Chem. Mater.* **2006**, *18*, 1945 – 1950.
[40] C. Artini, M. Pani, A. Lausi, R. Masini, G. A. Costa, *Inorg. Chem.* **2014**, *53*, 10140 – 10149.
[41] C. Artini, G. A. Costa, M. Pani, A. Lausi, J. Plaisier, *J. Solid State Chem.* **2012**, *190*, 24 – 28.
[42] R. D. Shannon, *Acta Crystallogr. Sect. A* **1976**, *32*, 751 – 767.
[43] S. J. Hong, A. V. Virkar, *J. Am. Ceram. Soc.* **1995**, *78*, 433 – 439.
[44] D. J. Kim, *J. Am. Ceram. Soc.* **1989**, *72*, 1415 – 1421.
[45] J.-G. Li, T. Ikegami, Y. Wang, T. Mori, *J. Am. Ceram. Soc.* **2003**, *86*, 915 – 921.
[46] J. G. Li, X. D. Li, X. D. Sun, T. Ikegami, T. Ishigaki, *Chem. Mater.* **2008**, *20*, 2274 – 2281.
[47] F. Auzel, *Chem. Rev.* **2004**, *104*, 139 – 173.
[48] *Upconversion Processes in Transition Metal and Rare Earth Metal Systems, D. R. Gamelin, H. U. Gudel in Topics in Current Chemistry*, **2000**, *vol 214*, pp 1 – 56.
[49] X. Y. Chen, E. Ma, G. K. Liu, *J. Phys. Chem. C* **2007**, *111*, 10404 – 10411.
[50] H. Guo, *J. Solid State Chem.* **2007**, *180*, 127 – 131.
[51] H. Guo, Y. Li, D. Wang, W. Zhang, M. Yin, L. Lou, S. Xia, *J. Alloys Compd.* **2004**, *376*, 23 – 27.
[52] S. Xiao, X. Yang, Z. Liu, X. H. Yan, *J. Appl. Phys.* **2004**, *96*, 1360 – 1364.
[53] M. Pollnau, D. R. Gamelin, S. R. Luthi, H. U. Gudel, M. P. Hehlen, *Phys. Rev. B* **2000**, *61*, 3337 – 3346.
[54] P. Goldner, F. Pelle, *Opt. Mater.* **1996**, *5*, 239 – 249.
[55] G. Y. Chen, H. J. Liang, H. C. Liu, G. Somesfalean, Z. G. Zhang, *J. Appl. Phys.* **2009**, *105*, 114315.
[56] S. Sivakumar, F. C. J. M. Van Veggel, P. S. May, *J. Am. Chem. Soc.* **2007**, *129*, 620 – 625.
[57] M. Nakayama, M. Martin, *Phys. Chem. Chem. Phys.* **2009**, *11*, 3241 – 3249.
[58] S. Sen, H. J. Avila-Paredes, S. Kim, *J. Mater. Chem.* **2008**, *18*, 3915 – 3917.
[59] N. J. Kim, J. F. Stebbins, *Chem. Mater.* **2007**, *19*, 5742 – 5747.
[60] C. Tiseanu, V. I. Parvulescu, M. Sanchez-Dominguez, M. Boutonnet, *J. Appl. Phys.* **2012**, *112*, 013521.
[61] C. Tiseanu, B. Cojocaru, D. Avram, V. I. Parvulescu, A. V. Vela-Gonzalez, M. Sanchez-Dominguez, *J. Phys. D* **2013**, *46*, 275302.
[62] N. Shehata, K. Meehan, M. Hudait, N. Jain, *J. Nanopart. Res.* **2012**, *14*, 1173.

Manuscript received: November 16, 2016
Revised: February 6, 2017
Final Article published: ■■ ■■, 0000

Lift it up: Er^{III} and Er^{III}–Yb^{III} based nanophosphors, hosted in a family of monophasic oxidic Ce^{IV}–Gd^{III} solid solutions, were prepared. The yield of the upconversion (UC) process is discussed in the framework of both established and novel alternative mechanisms. Vacancies and the symmetry of the Er^{III} environment play major roles in the UC emission mechanisms.

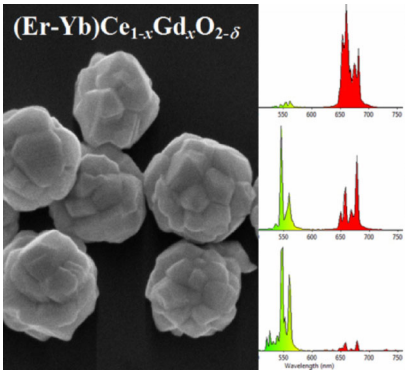

C. Sorbello, P. Gross, C. A. Strassert, M. Jobbágy, B. C. Barja**

■■ – ■■

Ce^{IV}–Gd^{III} Mixed Oxides as Hosts for Er^{III}-Based Upconversion Phosphors

These are not the final page numbers! ↗↗